

2012

Coupled electromagnetic and heat transfer model for microwave heating in domestic ovens

Krishnamoorthy Pitchai

University of Nebraska at Lincoln, s-kpitcha1@unl.edu

Sohan Birla

University of Nebraska-Lincoln, sbirla2@unl.edu

Jeyamkondan Subbiah

University of Nebraska-Lincoln, jeyam.subbiah@unl.edu


D. D. Jones

University of Nebraska-Lincoln, david.jones@unl.edu

Harshanardhan Thippareddi

University of Nebraska-Lincoln, harsha15@uga.edu

Follow this and additional works at: <http://digitalcommons.unl.edu/foodsciefacpub>

 Part of the [Bioresource and Agricultural Engineering Commons](#), [Electrical and Electronics Commons](#), [Food Processing Commons](#), [Other Engineering Science and Materials Commons](#), [Other Food Science Commons](#), and the [Power and Energy Commons](#)

Pitchai, Krishnamoorthy; Birla, Sohan; Subbiah, Jeyamkondan; Jones, D. D.; and Thippareddi, Harshanardhan, "Coupled electromagnetic and heat transfer model for microwave heating in domestic ovens" (2012). *Faculty Publications in Food Science and Technology*. 135.

<http://digitalcommons.unl.edu/foodsciefacpub/135>

This Article is brought to you for free and open access by the Food Science and Technology Department at DigitalCommons@University of Nebraska - Lincoln. It has been accepted for inclusion in Faculty Publications in Food Science and Technology by an authorized administrator of DigitalCommons@University of Nebraska - Lincoln.

Coupled electromagnetic and heat transfer model for microwave heating in domestic ovens

K. Pitchai^a, S.L. Birla^a, J. Subbiah^{a, b}, D. Jones^a, H. Thippareddi^b

a. Department of Biological Systems Engineering, University of Nebraska-Lincoln, NE 68583, United States

b. Department of Food Science and Technology, University of Nebraska-Lincoln, NE 68583, United States

Corresponding author – J. Subbiah, 212, L.W. Chase Hall, East Campus, University of Nebraska-Lincoln, NE 68583-0726, USA
Tel.: +1 402 472 4944; fax: +1 402 472 6338, email jsubbiah2@unl.edu

Abstract

Microwave ovens are used extensively for heating a variety of not-ready-to-eat food products. Non-uniform heating of foods in microwave ovens is a major concern in assuring microbiological safety of such products. The non-uniform heating of foods is attributed by complex interaction of microwaves with foods. To understand this complex interaction, a comprehensive model was developed to solve coupled electromagnetic and heat transfer equations using finite-difference time-domain based commercial software. The simulation parameters, cell size, heating time step, and number of iterations for steady state electromagnetic field were optimized. The model was validated by 30 s heating profile of a cylindrical model food (1% gellan gel) in a 700 W microwave oven. The model was validated qualitatively by comparing the simulated temperature profiles on three planes in the gel and compared them to the corresponding thermal images. Quantitative validation was performed by comparing simulated temperature of the gel at 12 locations with experimental temperature acquired at those points using fiber optic sensors. Simulated spatial temperature profiles agreed well with the thermal image profiles. The root mean square error values ranged from 0.53 to 4.52 °C, with an average value of 2.02 °C. This study laid a framework for selecting the required model parameters which are critical for better temperature prediction. The developed model can be effectively used to identify hot and cold spots in food products, thereby helping in microwavable food product development to achieve better cooking performance in terms of heating uniformity, food quality and safety. The model can also be used to identify the best product, package and cavity parameters to achieve better heating uniformity and electromagnetic distribution inside the cavity.

Keywords: Microwave heating, Modeling, Finite-difference time-domain method, Heat transfer, Thermal image, Fiber-optic thermocouples

1. Introduction

Because of rapid and convenient heating offered by microwave (MW) ovens, they have become a favorite kitchen appliance worldwide. Recent foodborne illness outbreaks and recalls associated with microwave heated packaged frozen foods have resulted in the food industry reviewing microwavable food product development. The main food safety issue with the not-ready-to-eat (NRTE) foods is their non-uniform heating in a domestic microwave oven. The non-uniform heating is due to: (1) interference of electromagnetic waves inside the microwave cavity resulting in hot and cold spots, and (2) variation in dielectric, physical, and thermal properties of food components during heating results in uneven absorption of microwave energy and subsequent heat dissipation. NRTE foods should be cooked thoroughly as some ingredients are not fully cooked and can be a source for the foodborne pathogens. Therefore, temperature uniformity is critical for ensuring safety of NRTE foods.

A drastic difference in dielectric properties of frozen ice and liquid water exasperates non-uniform heating of frozen foods heated in a microwave oven. Typically, frozen portion of the food absorb considerably less MW energy than the thawed food portion, because dielectric properties of ice are much less than that of liquid water ([Chamchong and Datta, 1999a]; [Chamchong and Datta, 1999b]). In microwave oven, electric field distribution is highly sensitive to changes in the dielectric and thermal properties of foods.

Current methods for designing of foods for microwave heating are mostly based on trial and error. A computer simulation of microwave heating of foods could facilitate proper designing of foods to assure microbial safety. Extensive modeling efforts have been made to simulate microwave heating using simple analytical approaches (Watanabe et al., 1978) to computational approaches solved using numerical methods. Researchers have made assumptions to simplify the problem and reduce the computational time. For example, instead of modeling

Nomenclature	
E	electric field (V/m)
ω	angular frequency (rads/s)
μ	permeability (H/m)
ϵ_0	free space permittivity (8.854×10^{-12} F/m)
ϵ	complex dielectric permittivity
H	magnetic field (H/m)
P_v	dissipated power density (W/m^3)
f	frequency (Hz)
\square	dielectric constant
ϵ''	dielectric loss factor
σ	electrical conductivity (S/m)
ρ	density (kg/m^3)
C_p	specific heat capacity at constant pressure ($J/g \text{ } ^\circ C$)
k	thermal conductivity ($W/m \text{ } ^\circ C$)
T	temperature ($^\circ C$)
h	convective heat transfer coefficient ($W/m^2/^\circ C$)
H_{old}	enthalpy of previous time step (J/cm^3)
H_{new}	enthalpy of current time step (J/cm^3)
P	microwave power output (W)
C_{pw}	specific heat of water ($4.186 J/g \text{ } ^\circ C$)
m_w	mass of water (g)
C_{pg}	specific heat of glass container ($0.55 J/g \text{ } ^\circ C$)
m_c	mass of glass container (g)
N	number of iterations needed for reaching a steady state
dt	electromagnetic time step (ns)
c	speed of light (3×10^8 m/s)
r	stability factor which should be ≥ 3
P_m	magnetron power (W)
S_{11}	reflection coefficient
NPA	normalized power absorption
a	effective cell size in meters (m)
T_p	simulated point temperature ($^\circ C$)
T_o	observed point temperature ($^\circ C$)

Maxwell's equation, several researchers simplified the problem by using Lambert's law, which calculates dissipated power by assuming that the energy decays in the food exponentially from the material surface to deep inside of the material ([Campanone and Zaritzky, 2005]; [Chamchong and Datta, 1999a]; [Chamchong and Datta, 1999b]; [Chen et al., 1993], [Khraisheh et al., 1997]; [Zhou et al., 1995]). Lambert's law does not represent the true electromagnetic field distribution inside the MW oven cavity (Datta & Anantheswaran, 2001). There have been several studies in literature comparing the Maxwell's and Lambert's law equations in predicting temperature during microwave heating of a frozen and model food ([Liu et al., 2005]; [Yang and Gunasekaran, 2004]). Liu et al. (2005) stated that although Lambert's law is not appropriate for microwave power processing, its simplified numerical results are comparable with the experimental methods. However, Maxwell's equations are more accurate than Lambert's law in calculating power dissipation in a food material (Yang and Gunasekaran, 2004).

Localized microwave heat dissipation in foods is diffused by conduction ([Basak and Ayappa, 1997]; [Ohlsson et al., 1974]). The dynamic physical situations cause rapid changes in material properties resulting in non-linear computational solution. Therefore, the non-linear problem of microwave heating needs to be solved by coupling electromagnetic and heat transfer equations. Models that couple electromagnetic and thermal equations to calculate temperature field of microwave-heated foods have been reported ([Dinčov et al., 2004]; [Geedipalli et al., 2007]; [Wäppling-Raaholt et al., 2002]; [Zhang and Datta, 2000]; [Zhang and Datta, 2003]). These models are solved iteratively using various numerical methods such as finite-difference time-domain (FDTD) (Tilford et al., 2007) and finite element method (FEM) ([Curcio et al., 2008]; [Zhang and Datta, 2000]).

Most of the microwave modeling research did not focus on optimizing the simulation parameters and describe the selection of the model parameters. Solving the electromagnetic equations require proper values of electromagnetic parameters such as frequency and electric field strength (Mechenova & Yakovlev, 2004). It is critical to develop a computer model that reduces susceptibility to numerical errors arising from poor discretization of time and space domain.

So far, researchers have assumed that a microwave oven is a cavity in which the port is located on the cavity wall ([Geedipalli et al., 2007]; [Dinčov et al., 2004]). In modern microwave ovens, geometric features such as metal bumps, dimples, and turntable crevices have been introduced to improve heating uniformity. Each of these features can dramatically change the

electric field distribution inside the cavity. Therefore, a simulation model should include all the features rather than considering the oven as a simple cavity with a waveguide.

Over the last two decades, with the availability of greater computational power and development of efficient numerical methods, computer simulation has become as a promising tool to understand microwave heating. In this study, a coupled electromagnetic (EM) and heat transfer model was developed using a Quickwave v7.5 (QWED Sp.z o.o., Warsaw, Poland) software based on FDTD method giving due consideration to each modeling parameters. The specific objectives of this study were to:

- develop a coupled electromagnetic and heat transfer model using FDTD based numerical method,
- optimize the electromagnetic and computational parameters of the developed model, and
- validate the developed model using a model food system.

Once the model is validated for this study, it will be expanded to include more features such as rotating turntable, phase change, and mass transfer in future studies.

2. Materials and methods

2.1. Model development

2.1.1. Governing equations

The microwave heating of a food material inside the oven is governed by a set of Maxwell's equations (Zhang and Datta, 2003).

$$\nabla \times E = j\omega\mu H \quad (1a)$$

$$\nabla \times E = -j\omega\epsilon_0\epsilon^*E \quad (1b)$$

$$\nabla \cdot (\epsilon E) = 0 \quad (1c)$$

$$\nabla \cdot H = 0 \quad (1d)$$

The oven cavity and waveguide walls were subjected to perfect electric conductors (PEC) boundary condition. An electromagnetic wave loses its energy when traveling through a lossy dielectric medium and part of the electromagnetic power is converted into thermal energy within the medium. Conversion of electromagnetic energy into thermal energy is governed by (Goldblith and Wang, 1967):

$$P_v = 2\pi f \epsilon_0 \epsilon'' E^2 \quad (2)$$

The dielectric loss in a material due to electric conductivity is given by

$$\epsilon'' = \frac{\sigma}{2\pi \epsilon_0 f} \quad (3)$$

The microwave dissipated power term is considered as source term in Fourier heat transfer equation.

$$\rho C_p \frac{\partial T}{\partial t} = k \nabla^2 T + P_v(x, y, z, t) \quad (4)$$

The surface of the food exchanges heat with surrounding air by convection expressed as

$$-k \frac{\partial T}{\partial n} - h(T - T_2) \quad (5)$$

When evaporative losses from the surface are significant, the evaporative loss term in heat transfer equations need to be included. In general, the evaporative loss is considered minimal when surface temperature of the food is below 70 °C and therefore was ignored in this study. Heat loss to the air from the load was approximated by assuming heat transfer coefficient value of 10 W/m²/°C which is quite often used in natural convective heat transfer in air (Tong and Lund, 1993). To make this assumption valid, we turned off the air going inside the cavity, which ensured that natural convection is taking place at the air-material interface. If the air flow goes into the cavity, then the simple convective heat transfer boundary is not valid on the entire air-object interface as the surfaces in front of the air will have higher heat transfer coefficient than the surfaces opposite to it (Verboven et al., 2003).

2.1.2. Geometric model

Geometric model was developed for a 700 W rated power (629 W available power measured using IEC 60705 method) microwave oven (Sharp Electronics Corp., New Jersey, USA). In the geometric model we included oven cavity, magnetron, turntable, waveguide, crevices (bottom of the cavity) and a metal bump as shown in Figure 1. The microwave feed port was located on top of one side of the microwave oven cavity. An electromagnetic wave travels with certain patterns (modes) in the waveguide governed by the frequency and waveguide dimensions. When the power is excited at one end of the waveguide, the electromagnetic waves would assume either traverse

electric (TE) or traverse magnetic (TM) modes depending on cross-section of the waveguide. So far, in the literature only TE (most often TE₁₀) and TM modes have been used to assign at port boundary assuming the waveguide is rectangular and infinitely long. In this study, we included magnetron as coaxial power source as shown in Figure 1 and compared results with input as TE₁₀ mode at the mouth of the waveguide.

2.1.3. Simulation strategy

Solving coupled non-linear Maxwell's equations and heat transfer equations requires iterative computational techniques to perform the simulation. QuickWave v7.5 (QWED, Poland) a commercial software was used for solving coupled equations. The calculated electric field strength is applied as an input to determine the dissipated power density using Eq. (2). In heat transfer analysis, new enthalpy fields are updated in every time step using the following relation:

$$H_{new}(x, y, z) = H_{old}(x, y, z) + P_v(x, y, z)\Delta t \quad (6)$$

The new temperature field in the medium is interpolated using the updated enthalpy.

$$T_{new}(x, y, z) = T[H_{new}(x, y, z)] \quad (7)$$

In the current time step, thermal properties of the medium are updated with respect to changes in the temperature field. As a sequence, new EM properties are calculated based on the new temperature field and are then used to calculate new electromagnetic fields and microwave power source term. This cyclical process continues until a desired heating time is reached.

2.1.4. Simulation parameters

A solution to the electromagnetic field is prone to numerical errors when appropriate simulation parameters are not set correctly. Therefore, it is critical to conduct a study to determine optimal simulation parameters to minimize the numerical errors. In this study, simulation variables such as number of iterations to reach steady state, cell size, heating time step, magnetron frequency, electric field strength, electromagnetic mode and power input were studied to identify their optimum values. The simulations were performed on a Dell Precision 690 workstation with an operating memory of 24 GB RAM running on quad-core Intel Xeon clocked at 2.93 GHz frequency processor.

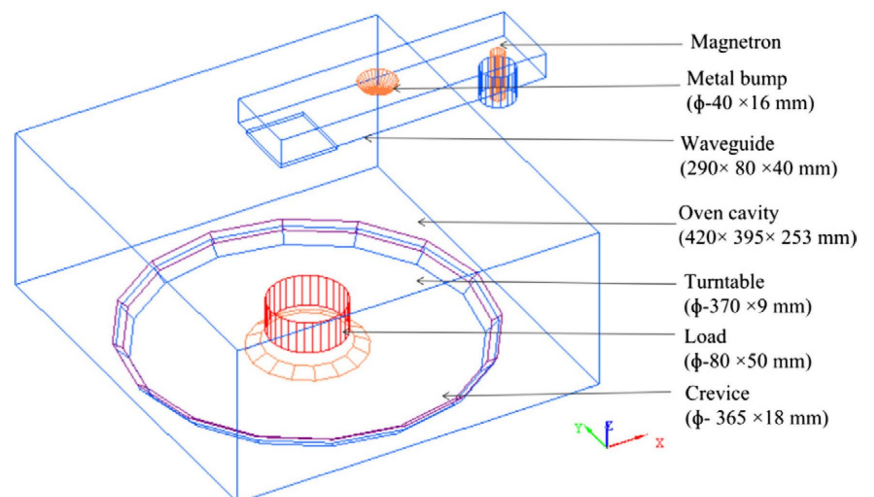


Figure 1. Geometric model of 700 W rated power microwave oven cavity with magnetron as coaxial microwave feed source.

2.2. Experimental procedure

2.2.1. Power output measurement

Power output of a magnetron is required to determine initial value of electric field strength at input port. The power delivered by the magnetron was indirectly determined using International Electrotechnical Commission (IEC) method. This method assumed that there is no reflection of microwave energy from the cavity and all the power delivered by the magnetron is fully absorbed by the 1000 g load (IEC, 1999). Three replications were performed with the interval of 6 h between replications allowing the magnetron to cool down to room temperature. The determined average microwave power output was 629 W, which is 90% of original rated power.

2.2.2. Model food preparation

A homogeneous, gellan gel cylinder (80 mm dia \times 50 mm height) was used for model validation. One percent gellan gum powder (Kelcogel, Kelco Division of Merck and Co., San Diego, CA), a fermented polysaccharide plant tissue powder, was gradually dissolved in deionized water and the solution temperature was raised to 90 °C in about 15 min. CaCl₂ (0.17 wt.%) was added to the hot gellan gum solution to form a firm gel. The hot solution was then poured into a cylindrical container and allowed to cool at room temperature for 30 min to ensure solid gel formation (Birla et al., 2008). The prepared gel was stored at \sim 4 °C in a closed container.

2.2.3. Dielectric and thermo-physical properties

The dielectric properties of 1% gellan gel were measured using an Agilent Technologies™ N5230A PNA-L Vector Network Analyzer (VNA) attached to an open-ended coaxial high-temperature probe (Agilent 85070E-020) with a two-port electronic calibration (ECal) module (Agilent, Model N4691-6004). Only one port of the VNA's was used and calibrated using the ECal module, and then the probe was subsequently calibrated using the references by following air/50 Ω short/deionized water protocol before each measurement session as described by Blackham and Pollard (2002). The VNA was configured to take 201 measurements linearly spaced between 10 and 3000 MHz frequency but values only at 2450 MHz were used in the simulation. A 30 g of gel was placed inside the stainless-steel jacketed test cell (20 mm inner-dia, 92 mm height) and the high-temperature probe for measuring dielectric properties was sealed in top of the test cell and kept in touch with the gel. The contact between the high-temperature probe and the gel during measurement was ensured by a spring-loaded stainless-steel piston on the bottom of the test cell. Dielectric properties were measured from 10 to 80 °C at every 10 °C interval. The sample temperature in the test cell was maintained by a programmable oil bath. Three replicates were carried out and average values were used for regression equations to be used in simulations. In addition to three samples as true triplicates, dielectric measurements were collected three times at each temperature and were averaged to improve signal-noise ratio. Table 1 summarizes the various properties of the gellan gel and glass turntable used in the model.

2.2.4. Model validation

The gellan gel samples stored in a refrigerator were removed from the container and left outside for 4 h to equilibrate to ambient temperature. A gel cylinder placed in the center of the stationary turntable was subjected to 30 s heating in a microwave oven. Transient temperature at 12 points was recorded using fiber-optic sensors (4-channel reflex signal conditioner, accuracy \pm 0.8 °C, Neoptix Inc., Quebec, Canada) as shown in Figure

2. Because, the instrument had only 4-channels to measure the temperatures, the experiments were repeated for three batches to get transient temperatures at 12 locations. To make sure all the 4-sensors are at same locations in each replication, a graduate thin rod was inserted from the top surface of the gel to the desired depth to make a hole which had the same diameter as the diameter of the fiber-optic sensor. Through those holes, the sensors were then inserted into the gel. This ensured that the sensors were properly placed at predefined locations in all replications. Immediately after MW heating, the thermal images of top and bottom of gel cylinder were taken using a thermal imaging camera (SC640, accuracy \pm 2 °C, 640 \times 480 pixels, FLIR systems, Boston, MA). Then, the sample was sliced horizontally in the middle (25 mm from top) to obtain image at the middle plane. The thermal imaging camera was calibrated to identify appropriate emissivity value. We placed the gel below the thermal imaging camera and adjusted the emissivity value until it matches the temperature measured by a thermocouple. He emissivity value was set at 0.95. In addition to emissivity value, the other image acquisition parameters such as distance between the lens and the object and ambient temperature were set constant for all images. A total of nine experiments (three replications \times three batch) were conducted to get the temperature profile of 12 locations. Experiments were carried out with the interval of 6 h to ensure the cold start of magnetron each time.

Table 1. Properties of 1% gellan gel and glass turntable used in the simulation.

Properties	Gellan gel	Glass ^c
Specific heat (kJ/kg °C)	4.16 ^a	0.55
Density (kg/m ³)	1010 ^a	2050
Thermal conductivity (W/m °C)	0.53 ^a	0.1
Dielectric constant at 2.45 GHz	-0.23T + 81.103 ^b	6
Dielectric loss factor at 2.45 GHz	0.0019T ² - 0.264T + 18.033 ^b	0

a. Birla et al. (2008).

b. In this study.

c. Quickwave (2008).

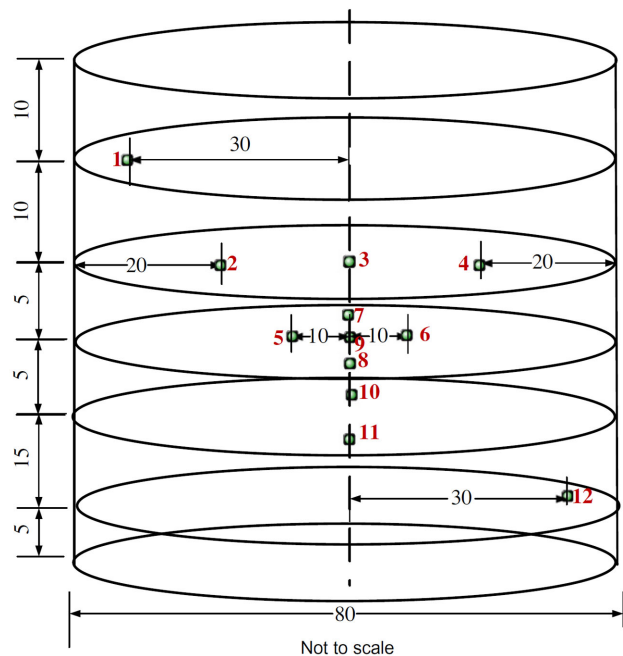


Figure 2. Location of the fiber-optic sensors in gellan gel cylinder.

3. Results and discussion

3.1. Model parameters

3.1.1. Iterations for electromagnetic steady state

The solution of electromagnetic equations requires a large number of iterations for obtaining steady state field at each time step. It is an important parameter for accurate prediction of temperature (Kopyt and Celuch, 2003). A criterion of converged electric field solution is the difference of electric field strength calculated at two consecutive iterations at any point in the domain should be less than 0.25% of the electric field strength calculated in previous iteration (Quickwave, 2008). In this study, four locations (1, 3, 9, and 12 of Figure 2) were chosen to study the electromagnetic steady state.

The electric field will stabilize with increasing iterations and therefore the temperature at any point in the domain will stabilize. In this study, simulations were carried out with increasing number of electromagnetic periods (N_p) (one period is equal to the time needed to complete one cycle of electromagnetic wave while propagating in medium = $1/\text{frequency} = 0.40$ ns) from 50 to 450 with the interval of 50 periods to find minimum number of periods needed for stable temperature. The relationship of electromagnetic periods (T_p) to the number of iterations (N) is described by the following relation:

$$N_p \times T_p = N \times dt \quad (8)$$

The electromagnetic time step, dt , is automatically calculated by the software by taking account of the smallest cell size in the computational domain to obey the Courant stability criteria as defined in Eq. (9). For a 3-D problem, the electromagnetic time step has to fulfill the following condition:

$$dt = \frac{a}{c \times r} \quad (9)$$

The electromagnetic time step was calculated as 0.00166 ns by the software.

The Eq. (8) was then used to determine the number of iterations for the corresponding period.

Figure 3 shows that with an increasing number of iterations, the temperature increases and reaches steady state after certain number of iterations which means that no significant change

in temperature occurs at all four selected locations in the load. After around 51,012 iterations, the change in temperature was negligible at the center of the model domain (location 9). In the other three locations in the domain, the temperature stabilized at around same iterations. Therefore, it was concluded that electromagnetic steady state has reached around 51,012 iterations and this value was used in the rest of the simulations.

3.1.2. Time step

Appropriate selection of time step is an important factor in balancing the computation time and accuracy of temperature prediction (Celuch et al., 2006). The choice of time step should be neither too big nor too small. In the case of a too big heating time step, immediate divergence of the temperature fields would occur, whereas in the case of too small, the convergence of temperature field would be reached but at the expense of longer simulation time. Therefore, to optimize heating time step, the simulations were performed for the total heating time of 30 s with time steps ranging from 1 to 30 s. Average dissipated power in the gellan gel load was calculated for each time step. Normalized power absorption (NPA) was defined as a ratio of average simulated dissipated power to the power absorbed by the 1000 g of water load experimentally calculated using IEC method (Zhang and Datta, 2003).

$$\text{NPA} = \frac{P_{\text{simulated}}}{P_{\text{IEC method}}} \quad (10)$$

When the value of NPA does not change with further refining of the time step, then the simulated temperature is considered to be independent of the time step. Figure 4 shows that increasing time steps from 4 to 30 s results in a decrease in the NPA value. Reducing the time step from 4 to 1 s does not change the NPA value considerably. Therefore, the time step could be selected somewhere between 4 and 1 s. In this study the gel dielectric properties does not change significantly over the short time span hence larger time can be taken. However, for materials undergoing phase change (frozen to thawing) time steps should be smaller. In this work, a time step of 2 s was further used in the simulations in order to have sufficient number of predicted temperature points to compare with experimental temperature profile.

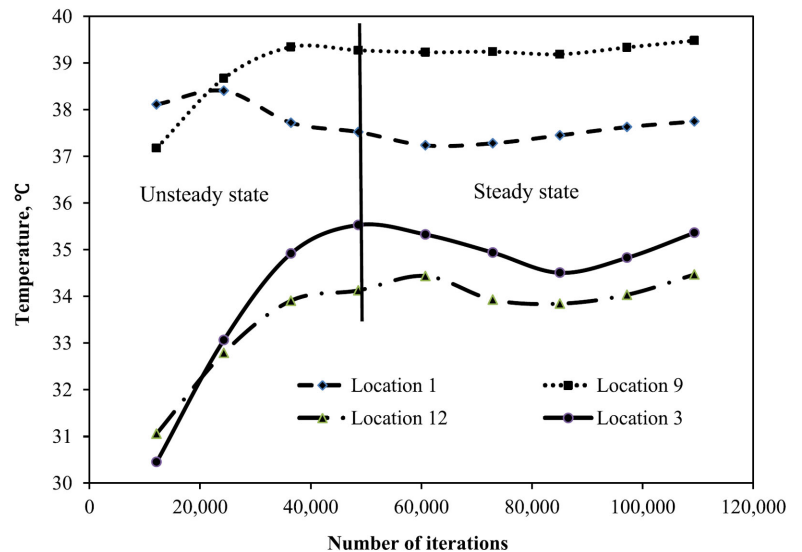


Figure 3. Optimization of electromagnetic steady state iterations at four locations in gellan gel.

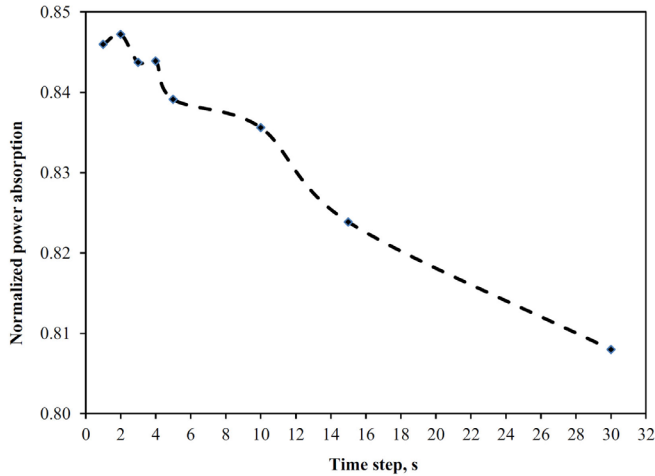


Figure 4. Effect of heating time step on power absorption.

3.1.3. Mesh size

Mesh size optimization is an important step in obtaining reasonable simulation results. Reducing the mesh size by half brings the space discretization errors down by a factor of four. However, it should also be mentioned that the computing time will increase by almost 16 times and memory requirement will increase by eight times (QuickWave, 2008). The QuickWave software manual suggests that 12 cells per wavelength in the domain ($\lambda = 12.22$ cm in air) is good enough for mesh independent results. The FDTD method rule of thumb (Eq. (11)) suggests using ten cells per wavelength in the dielectric medium (Pathak et al., 2003).

$$\text{Cellsize, } m \leq \frac{c}{10f\sqrt{\epsilon}} \quad (11)$$

Electromagnetic simulation in a dielectric material (gellan gel in this study) typically requires about 8–10 cells per wavelength (QuickWave, 2008). But, the exact number of cells to be adopted in the computation domain is critical in minimizing the computational speed. The wavelength of microwaves in gel is 13 mm and therefore the cell size should be less than 1.3 mm. In this study, cell size in the air domain was set at 5 mm (for example, cavity size in x direction is 395 mm which gave 79 cells in air). Figure 5 shows the meshing scheme used in this study in 2-dimensional direction in x - y (top view) and y - z (side view) planes. In the gellan gel domain, the effect of cell size along the x , y and z direction in the range of 1–6 mm on power absorption was studied. The simulations were performed with 2.45 GHz frequency sinusoidal excitation (meaning that EM wave had a single frequency) to study the effect of cell size on the normalized power absorption. Figure 6 shows the effect of cell size on normalized power absorption in the gel. The cell size interval from 1 to 3 mm did not have much variation in microwave power absorption. However, the normalized power absorption in the load drops drastically from 0.78 to 0.64 when cell size changes from 4 mm to 5 mm cell size. Table 2 summarizes the information of number of cells, memory required, normalized power absorption, and % difference. Changing the cell

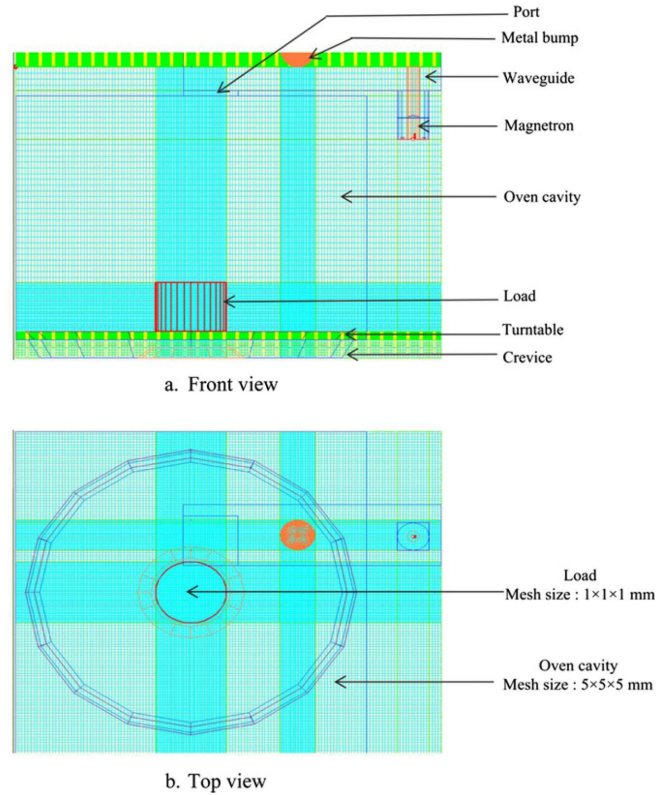


Figure 5. Meshing scheme in the computational domain.

size from 1 to 3 mm provided more or less the same normalized power absorption and percent difference error was much smaller than 2% (Table 2). However, the normalized power absorption calculated for 1 mm (0.84) was slightly higher than the NPA at 2 and 3 mm (0.83 and 0.81, respectively). In this study, 1 mm cell size in gellan gel was selected for model validation.

3.1.4. Electromagnetic mode

Scattering parameter, S_{11} , (a measure of reflected power to the magnetron power from the cavity) was also simulated in a frequency range of 2.4–2.5 GHz. This frequency range covers the magnetron frequency spectrum. The dimensions of the port, used in this study, allow either TEM or TE_{10} modes and will not allow the TM mode to develop. Therefore, both TEM and TE_{10} modes were evaluated in this study. Figure 7 compares the simulated scattering parameters calculated using two input port conditions namely coaxial feed (TEM) and TE_{10} mode. In case of the TE_{10} mode, the reflected power is slightly higher than that of TEM mode throughout the frequency spectrum. It gives the indication that the electromagnetic energy couples much better in TEM mode than TE_{10} mode with the load. Interestingly, the deep resonance (least value of S_{11}) was found to occur at the same frequency, which is at 2.46 GHz in both types of feed conditions. Besides, the coaxial feeding in a microwave oven represents actual scenario. Therefore, in this study TEM mode was used for model validation.

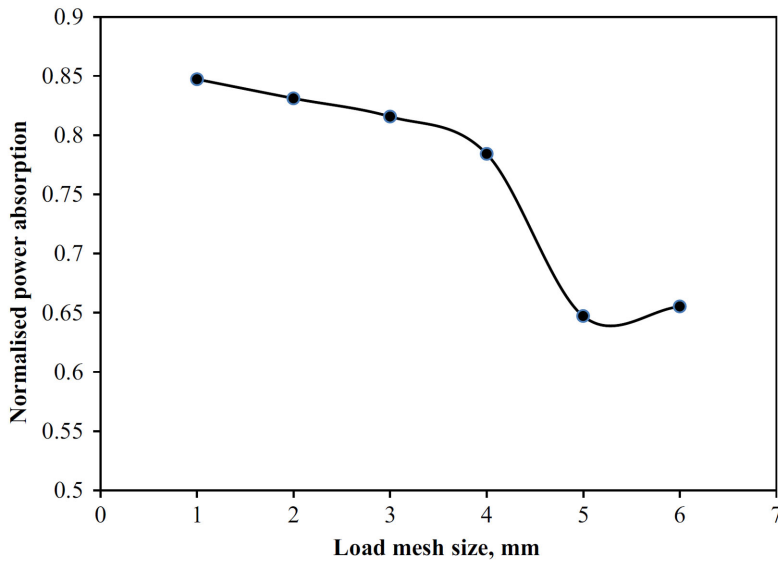


Figure 6. Effect of mesh refinement on absorption of microwave power.

Table 2. Effect of mesh refining on absorbed power in the gel.

Mesh size (mm)	Number of cells	Memory required (MB)	Normalized power absorption	% Difference
1	4661,376	445	0.847	-
2	2341,911	223	0.831	1.92
3	1803,100	172	0.816	1.87
4	1555,827	148	0.784	3.95
5	1413,720	135	0.647	19.14
6	1353,807	129	0.655	1.23

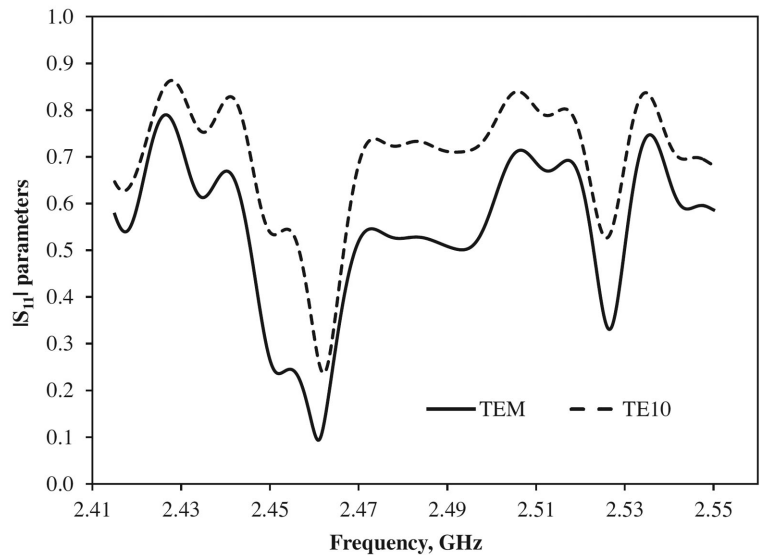
3.1.5. Electric field strength

The magnetron output frequency and power depend on the impedance of the heating load placed on the turntable. It is essential to know the exact magnetron power output for providing correct value of electric field strength at the feeding port. Value of electric field strength was estimated by an formula (Soltysiak et al., 2008):

$$E = \sqrt{\frac{2 \times P_m}{(1 - |S_{11}|^2)}} \tag{12}$$

The impedance mismatch of the load leads to reflect some energy back to the magnetron, which can be seen in the plot of scattering parameter versus frequency (Figure 7). The original IEC standard suggests using 1000 g of water load. As the gel mass was 250 g, the IEC method was modified to calculate microwave power absorption in 250 g of water load, which had the same 0.17% salt content as that of the gellan gel. The microwave power calculated for 250 g of water load was 508.11 W. The S_{11} parameter extracted for 250 g of water as a function of frequency is shown in Figure 8. The deepest resonance for this load size was found at 2.458 GHz frequency ($S_{11} = 0.243$). Using Eq. (12), the electric field strength (E_1) was calculated as 32.90 V/cm for 250 g water load at 2.458 GHz frequency.

Figure 7. Scattering parameter of TEM and TE₁₀ electromagnetic modes extracted from frequency spectrum.



To confirm that the electric field strength value calculated using Eq. (12), the calculated electric field strength (E_1) at 2.458 GHz frequency was used to simulate 250 g of water and power absorbed in the water load was calculated from simulation results. The calculated power can then be used to adjust the electric field strength so that the new electric field strength will make the simulation energy absorbed by the load equal to the energy absorbed by the load measured experimentally using the modified IEC method. As power is proportional to the square of the electric field strength, the following relationship was used to determine the new electric field strength so that simulated energy absorbed by the load matches the value determined experimentally. The original electrical field strength ($E_1 = 32.90$ V/cm) used in the simulation resulted in the power absorption ($P_{simulated}$). The new electric field strength (E_2) was determined to match the power determined by modified IEC method ($P_{IEC\ method}$) was calculated using the following relationship:

$$\frac{P_{IEC\ method}}{P_{simulated}} = \frac{E_2^2}{E_1^2} \quad (13)$$

The calculated (E_2) value was then used in the gellan gel simulation. The above correction procedure was repeated for different frequencies, because the power absorption and reflecting power varies with magnetron operating frequency.

3.1.6. Magnetron frequency

Initially, monochromatic frequency of 2.458 GHz was used as input to the model with sinusoidal waveform excitation; however mismatch of predicted and observed temperature profiles prompted us to evaluate the effect of frequencies on the heating pattern. The instantaneous frequency emitted by a magnetron in a microwave oven depends on two parameters: cathode-anode voltage and the high frequency output impedance of the magnetron which is set by the load (Ghammaz et al., 2003). Changes in dielectric properties with temperature causes change in the load impedance, which in turn shifts the frequency of the magnetron. The frequency shift not only changes the heating rate but also changes the field distribution (Celuch and Kopyt, 2009). A typical magnetron operating frequency deviates at about 50 MHz (Yakovlev, 2006).

Figure 8 shows that the deep resonance occurred at 2.458 MHz for the gel cylinder. Stipulated frequency is

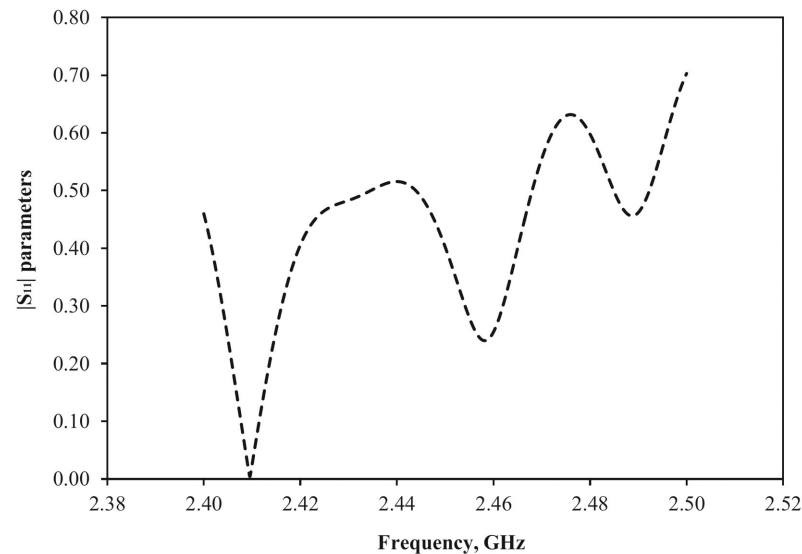


Figure 8. Scattering parameter of TEM extracted from frequency spectrum for 250 g of water load.

2.45 GHz for household magnetrons. Therefore, the computer simulations were performed with sinusoidal excitation for three monochromatic frequencies: 2.450, 2.455, and 2.458 GHz individually. Simulated temperature profiles obtained for these frequencies were compared with the experimental temperature profiles and root mean square error (RMSE) was calculated as:

$$RMSE = \sqrt{\frac{1}{n} \sum_{i=1}^n (T_p - T_0)^2} \quad (14)$$

Figure 9 shows the spatial temperature profiles collected at three planes for the three frequencies (2.45, 2.455 and 2.458 GHz) when compared with the experimental profile. It is quite evident from Figure 9 that locations of hot and cold spots changes with change in magnetron frequency. Therefore, the magnetron input frequency spectrum should be taken into account for obtaining precise results.

3.2. Model validation

After establishing the model and selecting the appropriate model simulation parameters, the simulated temperature profiles were compared with the experimental profiles.

Table 3 shows model parameters used for validation study.

3.2.1. Spatial temperature profile

Spatial simulated temperature profiles of the gellan gel cylinder at three planes ($z = 0, 25,$ and 50 mm) were compared with experimental heating profiles obtained using the thermal imaging camera. Figure 9 shows the simulated and experimental temperature profiles obtained at three planes. It is evident that simulated temperature profiles were slightly higher than the experimental profiles. The cause of the error could be due to the time lapse between end of heating and imaging. However, the heating patterns of experimental profiles at top ($z = 0$ mm) and bottom ($z = 50$ mm) planes match those with the simulated profiles at 2.45 GHz frequency. The experimental middle image ($z = 25$ mm) seems to have a smudge effect due to slicing of the gellan gel sample. Because of the smudge effect, heating pattern in the middle thermal image implies more uniform heating. Zhang and Datta (2000) developed a coupled electromagnetic and heat transfer model for microwave heating of potato cylinder to 15 s heating. They had collected spatial temperature

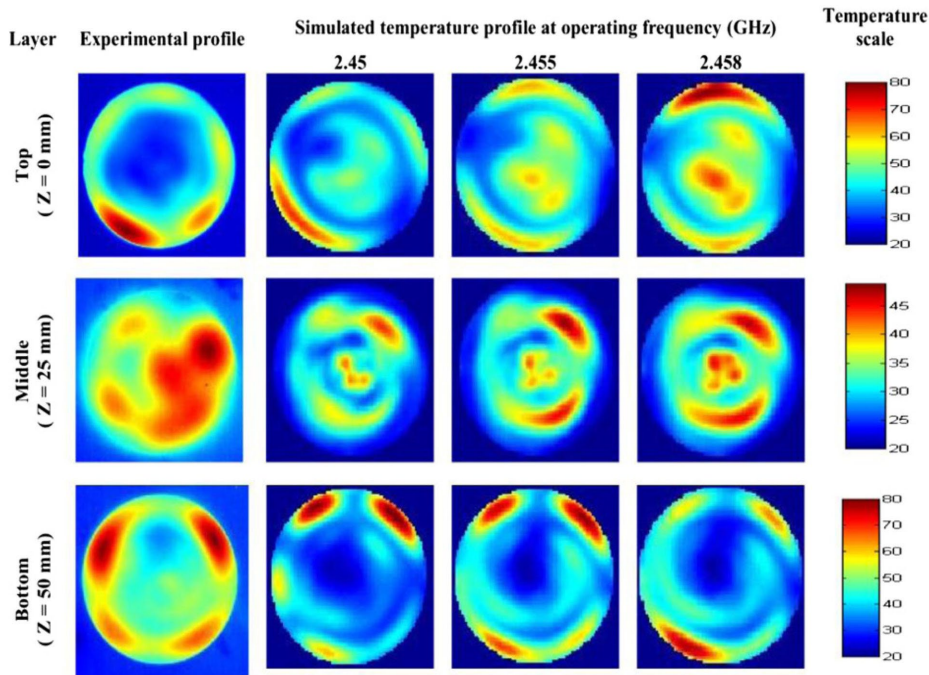


Figure 9. Effect of frequency on spatial heating profile of gellan gel cylinder (80 × 50 mm) subjected to 30 s heating in 700 W microwave oven.

Table 3. Selected simulation parameters.

Parameters	Optimized value
EM steady state iterations	36,450
Heating time step	2 s
Mesh size	Air: ($\Delta x = \Delta y = \Delta z = 5$ mm) Gel: ($\Delta x = \Delta y = \Delta z = 1$ mm)
Feed port mode	TEM
Frequency	2.45 GHz
Electric field strength	35.69 V/cm

profiles at three planes (top, middle and bottom). The predicted spatial profiles of their study at top and bottom planes heating pattern were not close to the experimental profiles. They reported that the maximum temperature difference at the top and bottom planes are 4 °C and 12 °C, respectively. The reason for not having the close match in heating patterns at the top and bottom planes is that when the temperature reaches above 70 °C, surface cooling effect would become dominant in high moisture food (more than 80% moisture content food). Gellan gel contains 99% water. However, in our study, when the temperature reaches above 70 °C (refer Figure 9), the predicted profiles at top and bottom planes are much closer to the experimental profiles, when compared to results reported by Zhang and Datta (2000). Thus, the indication of temperature in top and bottom planes (refer Figure 9) reaches above 70 °C, evaporative loss term should be included in the physics to get even better prediction. Similarly, Wäppling-Raaholt et al. (2002) developed a combined electromagnetic and heat transfer model for heating a rectangular model (TX 151 gel) food to 50 s in microwave combination ovens. Even though, they reported that the maximum temperature achieved in the top plane using simulation agreed well with the maximum temperature observed on the thermal image, the observed temperature pattern on the top plane was profoundly different from the simulated profile. Overall, spatial profiles calculated in this study are closer (in terms of maximum temperature and heating patterns) to the experimental thermal images than these two previous studies.

3.2.2. Transient-temperature profile

Transient temperature profiles obtained using fiber-optic sensors at 12 discrete points were compared with the simulated temperature profiles. Figure 10 compares the observed and simulated temperature profiles at six locations. The root mean square error (RMSE) value was calculated using Eq. (14) for each location. Standard deviations of three experimental replications calculated for each discrete time point was plotted in the graph. The RMSE values and end temperature difference calculated for 12 locations at three frequencies (2.45, 2.455, and 2.458 frequency) are given in Table 4. Those 12 locations were grouped into three categories based on their location in the load. The average RMSE values were lowest at 2.455 GHz, while it was slightly higher at 2.45 GHz. The spatial temperature profiles at 2.45 GHz were closely matched with the experimental profiles matched more closely to experimental profiles (Figure 9) and therefore further discussion on temporal profiles is done only for the 2.45 GHz frequency simulation. The average RMSE for the top layer ($n = 4$; $z = 10$ – 20 mm) temporal profiles were 2.15 °C \pm 1.76 °C, whereas, the average RMSE at middle plane ($n = 5$; $z = 25$ mm) and bottom layer ($n = 3$; $z = 30$ – 45 mm) were 2.08 °C \pm 1.34 °C and 1.79 °C \pm 0.89 °C, respectively (Table 4). The RMSE for points close to the top surface (location 1, $z = 10$ mm) was 4.52 °C. In the center of the model domain (location 9), the predicted profile was close to the observed profile with a RMSE value of 1.04 °C. The predicted profile at this location falls within the experimental variation throughout heating time. Some of the errors in model predictions can be attributed to the errors in maintaining the same consistent probe locations during heating and also for all replications. This, in fact, is the biggest problem in the microwave model validation studies, because a small error in placing the probes in the sample might result in radical changes in the temperature variation due to the dramatic variation of electrical field inside the cavity. In addition, discrepancies in experimental and simulated temperature can be attributed by assumption of mono-frequency of the magnetron. In reality magnetron operated in bandwidth of 50 MHz around 2.45 GHz central frequency and the exact central frequency and bandwidth would

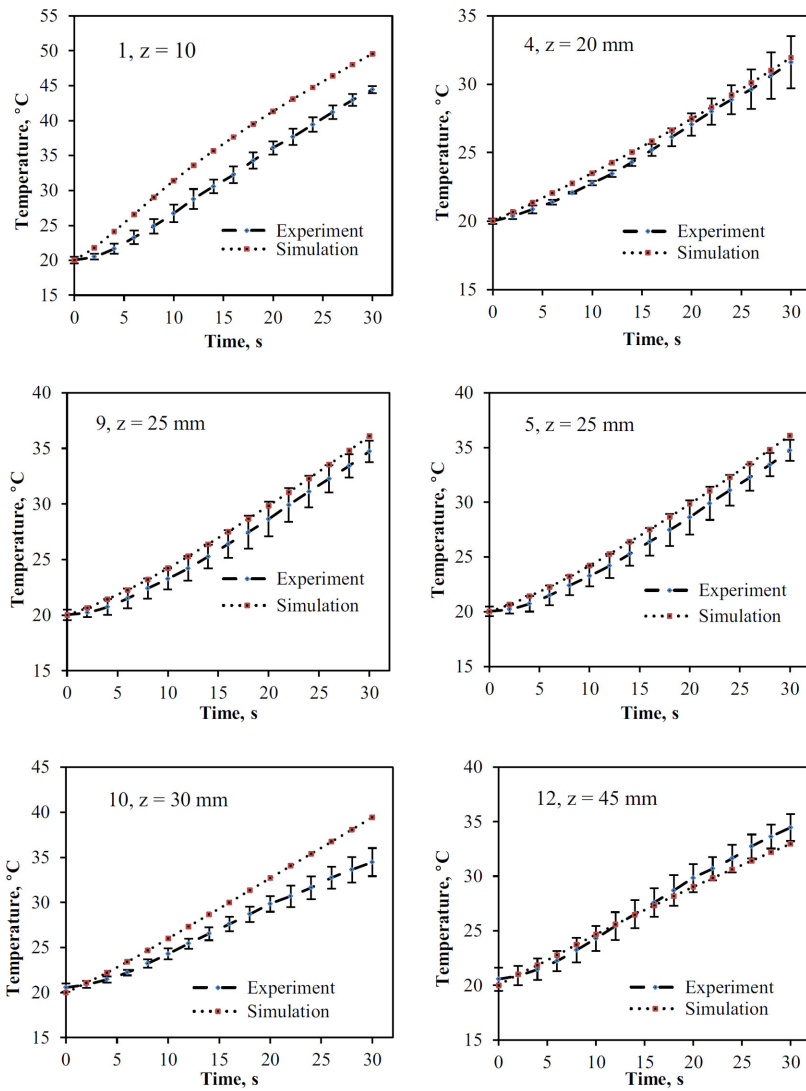


Figure 10. Simulated and observed time-temperature profile at six locations of gellan gel subjected at 2.45 GHz frequency.

Table 4. Comparison between transient experimental and predicted temperature using 2.45, 2.455 and 2.458 GHz magnetron frequency.

Layer position	Sensor position from top (mm)	Sensor ID	2.45_ RMSE (°C)	2.455_ RMSE (°C)	2.458_ RMSE (°C)
Top	10	1	4.52	3.85	4.04
	20	2	2.37	1.23	0.28
	20	3	1.16	1.77	2.39
	20	4	0.53	0.24	0.67
	Avg.	2.15	1.77	1.85	
Middle	25	5	0.81	0.74	1.22
	25	6	4.18	2.46	1.25
	25	7	1.99	1.72	1.18
	25	8	2.36	1.59	0.52
	25	9	1.04	2.83	4.63
Avg.	2.08	1.87	1.76		
Bottom	30	10	2.76	4.62	6.32
	30	11	1.82	1.38	2.21
	45	12	0.78	1.57	0.45
	Avg.		1.79	2.52	2.99
Global average			2.02	2.00	2.09

change with coupling with various loads. Evaporative cooling was not considered in this model and might have slightly contributed to minor errors in prediction. Tilford et al. (2007) developed a simulation model to predict the transient temperature profiles in cheesy sauce at eight locations of the food. In their study, the predicted temporal profiles were close to the observed profiles only in shorter heating time (15 s) and then temperature deviations were large for longer heating time. Given complex nature of microwave heating, overall model predictions were reasonably good.

3.2.3. End temperature comparison

The final temperature reached in simulation is an important value in food safety issues, because microbial inactivation rate is much faster at higher temperatures than at lower temperatures. Table 5 shows the final temperature difference calculated at 12 locations. At 2.45 GHz frequency, the average final temperature difference at the top plane ($n = 4; z = 10-20$ mm) was $2.82 \text{ }^\circ\text{C} \pm 2.04 \text{ }^\circ\text{C}$, whereas, the average final temperature difference at the middle plane ($n = 5; z = 25$ mm) and bottom plane ($n = 3; z = 30-45$ mm) were $3.85 \text{ }^\circ\text{C} \pm 2.63 \text{ }^\circ\text{C}$ and $3.30 \text{ }^\circ\text{C} \pm 1.74 \text{ }^\circ\text{C}$, respectively (Table 5). It is important to evaluate whether the model over-predicts or under predicts temperature at various locations to provide guidelines for microbial inactivation studies. The negative sign indicates over-prediction,

Table 5. End temperature difference of simulated (2.45 GHz frequency) and observed temperature after 30 s of microwave heating.

Layer position	Sensor position from top (mm)	Sensor ID	$T_{\text{experiment}}$ (°C)	$T_{\text{simulated}}$ (°C)	ΔT (°C)
Top	10	1	44.43	49.57	-5.13
	20	2	33.73	30.12	3.61
	20	3	27.2	29.42	-2.22
	20	4	31.60	31.95	-0.35
Middle	25	5	33.23	31.31	1.92
	25	6	36.06	28.01	8.06
	25	7	31.83	27.89	3.95
	25	8	31.10	27.08	4.02
	25	9	34.73	36.09	-1.36
Bottom	30	10	34.46	39.44	-4.97
	30	11	27.20	30.64	-3.44
	45	12	34.46	32.97	1.50

$\Delta T = (T_{\text{experiment}} - T_{\text{simulated}})_{\text{final}}$. Italicized numbers denote over-prediction; normal numbers denote under-prediction.

whereas positive sign indicates under-prediction. In top and bottom plane, most (5 out of 7) of the locations, the model over-predicted the temperature. On the other hand, in middle plane ($n = 5$; $z = 25$ mm) the model under predicted at 4 out of 5 locations. By increasing the heat transfer coefficient value at the interface of dielectric material (gel) and air, over-prediction at top plane would be reduced to get more close prediction.

4. Potential applications of the model in food industry

The developed model can be used in the food industry to identify the hot and cold spots locations in food product developed during microwave heating. Besides, the model can be used effectively in microwave food product development where the model enables the users to identify the best food and package design parameters to achieve better heating uniformity using simulation. Thus the model guides the food industry in developing food products with better cooking performance in various microwave ovens that results in better food quality and safety. The model can also help in developing cooking instructions. The model can play a vital role in microwave cavity design by assisting design engineers to achieve more uniform electromagnetic distribution within the cavity.

5. Conclusions

A comprehensive coupled electromagnetic and heat transfer model was developed to simulate microwave heating in domestic oven. The conformal FDTD based numerical method was used to solve electromagnetic Maxwell's equations and Fourier heat transfer equations. Effects of various electromagnetic and computational parameters were studied and the procedure for selecting appropriate value for each parameter was discussed. The microwave heating of a gellan gel cylinder was simulated using the optimized parameters for validation of the model. Simulated spatial and temporal profiles using 2.45 GHz were found in good agreement with experimental temperature

profiles. The predicted transient temperature profiles were close to the observed temperature profiles with the RMSE value of 2.15 °C, 2.08 °C and 1.79 °C at the top, middle, and bottom planes, respectively.

Acknowledgment – The authors gratefully acknowledge the financial support provided by the USDA CSREES – NIFSI Grant (Project Number: 2008-51110-04340).

References

- Basak, T., Ayappa, K.G., 1997. Analysis of microwave thawing of slabs with effective heat capacity method. *AIChE Journal* 43 (7), 1662–1674.
- Birla, S.L., Wang, S., Tang, J., Tiwari, G., 2008. Characterization of radio frequency heating of fresh fruits influenced by dielectric properties. *Journal of Food Engineering* 89 (4), 390–398.
- Blackham, D.V., Pollard, R.D., 2002. An improved technique for permittivity measurements using a coaxial probe. *IEEE Transactions on Instrumentation and Measurement* 46 (5), 1093–1099.
- Campanone, L.A., Zaritzky, N.E., 2005. Mathematical analysis of microwave heating process. *Journal of Food Engineering* 69 (3), 359–368.
- Celuch, M., Kopyt, P., 2009. Modeling microwave heating in foods. In: Lorence, M.W., Peshek, P.S. (Eds.), *Development of Packaging and Products for use in Microwave Ovens*. Woodhead Publishing Limited, Cambridge, UK, p. 408.
- Celuch, M., Gwarek, W.K., Sypniewski, M., 2006. A novel FDTD system for microwave heating and thawing analysis with automatic time-variation of enthalpy-dependent media parameters. *Advances in Microwave and Radio, Frequency Processing*, 199–209.
- Chamchong, M., Datta, A.K., 1999a. Thawing of foods in a microwave oven: I. Effect of power levels and power cycling. *Journal of Microwave Power and Electromagnetic Energy* 34 (1), 9–21.
- Chamchong, M., Datta, A.K., 1999b. Thawing of foods in a microwave oven: II. Effect of load geometry and dielectric properties. *Journal of Microwave Power and Electromagnetic Energy* 34 (1), 22–32.
- Chen, D.S.D., Singh, R.K., Haghighi, K., Nelson, P.E., 1993. Finite element analysis of temperature distribution in microwaved cylindrical potato tissue. *Journal of Food Engineering* 18 (4), 351–368.
- Curcio, S., Aversa, M., Calabruno, V., Iorio, G., 2008. Simulation of food drying: FEM analysis and experimental validation. *Journal of Food Engineering* 87 (4), 541–553.
- Datta, A.K., Anantheswaran, R.C., 2001. *Handbook of Microwave Technology for Food Applications*. CRC Press, Berlin.
- Dinčov, D., Parrott, K., Pericleous, K., 2004. A new computational approach to microwave heating of two-phase porous materials. *International Journal of Numerical Methods for Heat and Fluid Flow* 14, 783–802.
- Geedipalli, S.S.R., Rakesh, V., Datta, A.K., 2007. Modeling the heating uniformity contributed by a rotating turntable in microwave ovens. *Journal of Food Engineering* 82 (3), 359–368.
- Ghammaz, A., Lefeuvre, S., Teissandier, N., 2003. Spectral behavior of domestic microwave ovens and its effects on the ISM band. *Annals of Telecommunications* 58 (7), 1178–1188.

- Goldblith, S.A., Wang, D.I.C., 1967. Effect of microwaves on *Escherichia coli* and *Bacillus subtilis*. *Applied and Environmental Microbiology* 15 (6), 1371.
- International Electrotechnical Commission (IEC), 1999. IEC Publication 60705:1999. Household Microwave Ovens – Methods for Measuring Performance. International Electrotechnical Commission, Geneva.
- Khraisheh, M.A.M., Cooper, T.J.R., Magee, T.R.A., 1997. Microwave and air drying I. Fundamental considerations and assumptions for the simplified thermal calculations of volumetric power absorption. *Journal of Food Engineering* 33 (1–2), 207–219.
- Kopyt, P., Celuch, M., 2003. FDTD modelling and experimental verification of electromagnetic power dissipated in domestic microwave ovens. *Journal of Telecommunications and Information Technology* 1, 59–65.
- Liu, C.M., Wang, Q.Z., Sakai, N., 2005. Power and temperature distribution during microwave thawing, simulated by using Maxwell's equations and Lambert's law. *International Journal of Food Science & Technology* 40 (1), 9–21.
- Mechenova, V.A., Yakovlev, V.V., 2004. Efficiency optimization for systems and components in microwave power engineering. *Journal of Microwave Power and Electromagnetic Energy* 39 (1), 15–30.
- Ohlsson, T., Bengtsson, N.E., Risman, P.O., 1974. The frequency and temperature dependence of dielectric food data as determined by a cavity perturbation technique. *Journal of Microwave Power and Electromagnetic Energy* 9 (2), 129–145.
- Pathak, S.K., Liu, F., Tang, J., 2003. Finite difference time domain (FDTD) characterization of a single mode applicator. *Journal of Microwave Power & Electromagnetic Energy* 38 (1), 37–41.
- QuickWave, 2008. Quickwave Editor and Simulator. QWED, Warsaw, Poland.
- Soltysiak, M., Erle, U., Celuch, M., 2008. Load curve estimation for microwave ovens: experiments and electromagnetic modelling. In: 17th IEEE International Conference on Microwaves, Radar and Wireless Communications, 2008. MIKON 2008, pp. 1–4.
- Tilford, T., Baginski, E., Kelder, J., Parrott, K., Pericleous, K., 2007. Microwave modeling and validation in food thawing applications. *The Journal of microwave power and electromagnetic energy* 41 (4), 30–45.
- Tong, C.H., Lund, D.B., 1993. Microwave heating of baked dough products with simultaneous heat and moisture transfer. *Journal of Food Engineering* 19 (4), 319–339.
- Verboven, P., Datta, A.K., Anh, N.T., Scheerlinck, N., Nicolai, B.M., 2003. Computation of airflow effects on heat and mass transfer in a microwave oven. *Journal of Food Engineering* 59 (2–3), 181–190.
- Wappling-Raaholt, B., Scheerlinck, N., Gait, S., Banga, J.R., Alonso, A., Balsa-Canto, E., VAN, I., 2002. A combined electromagnetic and heat transfer model for heating of foods in microwave combination ovens. *Journal of Microwave Power and Electromagnetic Energy* 37 (2), 97–111.
- Watanabe, M., Suzuki, M., Ohkawa, S., 1978. Analysis of power density distribution in microwave ovens. *Journal of Microwave Power and Electromagnetic Energy* 13 (2), 173–182.
- Yakovlev, V.V., 2006. Examination of contemporary electromagnetic software capable of modeling problems of microwave heating. *Advances in Microwave and Radio Frequency Processing*, 178–190.
- Yang, H.W., Gunasekaran, S., 2004. Comparison of temperature distribution in model food cylinders based on Maxwell's equations and Lambert's law during pulsed microwave heating. *Journal of Food Engineering* 64 (4), 445–453.
- Zhang, H., Datta, A.K., 2000. Coupled electromagnetic and thermal modeling of microwave oven heating of foods. *The Journal of microwave power and electromagnetic energy* 35 (2), 71–85.
- Zhang, H., Datta, A.K., 2003. Microwave power absorption in single-and multipleitem foods. *Food and Bioproducts Processing* 81 (3), 257–265.
- Zhou, L., Puri, V.M., Anantheswaran, R.C., Yeh, G., 1995. Finite element modeling of heat and mass transfer in food materials during microwave heating-Model development and validation. *Journal of Food Engineering* 25 (4), 509–529.